

# Particle identification by laser-induced incandescence in a solid-state laser cavity

Michelle Stephens, Nelson Turner, and Jon Sandberg

The laser-induced incandescence of a particle of unknown size and composition can be detected simultaneously with the light elastically scattered by the particle, providing information on both the size and composition of the particle. The technique relies on vaporization of the particle; detection of the incandescence signal at the time of vaporization allows determination of the boiling point of the particle, which can in turn be related to the composition of the particle. The elastically scattered signal provides information about the size of the particle and confirmation that it was vaporized. The technique is demonstrated by directing particles through a Nd:YAG laser cavity with  $\sim 10^6$  W/cm<sup>2</sup> of circulating intensity. Elements such as tungsten, silicon, and graphite, as well as common aerosols such as soot, can be detected and identified. © 2003 Optical Society of America

OCIS codes: 010.1100, 010.1120, 010.1280, 120.0120, 290.5850.

## 1. Introduction

Real-time measurement of the size and composition of airborne particles is important for clean-room evaluation, in-line vacuum monitoring, and environmental-pollutant detection. Information about the size of airborne particles in the 0.1–1- $\mu$ m-diameter range is readily obtained with commercially available systems that relate the magnitude of the elastically scattered light to the particle size.<sup>1,2</sup> Data about the composition of airborne particles can be obtained through time-of-flight mass spectrometry,<sup>3,4</sup> molecular spectroscopy,<sup>5</sup> and off-line through microscopical analysis; however, these techniques are not well-suited to applications involving low concentrations of particles. This work demonstrates the use of laser-induced incandescence (LII) simultaneously with a measurement of elastically scattered light to concurrently determine the size and boiling point of a single airborne particle.

LII has been used for combustion diagnostics and to study the chemistry of soot formation for many

years.<sup>6–14</sup> Two-color optical pyrometry has been used in conjunction with LII to measure the temperature of particles,<sup>15–17</sup> and it has also been used in conjunction with elastic-scattering measurements, laser doppler vibrometry, and other LII techniques to simultaneously determine the size, velocity, and temperature of soot particles.<sup>18,19</sup> However, this work is, to our knowledge, the first to demonstrate a method for using LII to provide information about the composition of an unknown particle. Other authors<sup>20–22</sup> have used LII to measure size distributions and concentrations of particles of different compositions but have not used the incandescence information to determine particle composition. Unlike many time-of-flight mass spectrometry systems, our system requires no heavy vacuum equipment and is easily portable.

In this demonstration a jet directs airborne particles through a Nd:YAG laser cavity. The intersection between the jet stream and the intracavity beam forms an interaction region in which light is both elastically scattered and absorbed by the incident particle. The absorbed light heats the particle so that it begins to incandesce. The intensity of the intracavity light is  $\sim 10^6$  W/cm<sup>2</sup>, which is enough to vaporize absorbing particles as they pass through the beam. Several detectors image the interaction region and detect the elastically scattered light as well as the incandescent light. The spectral bandwidth over which the incandescent light is detected can be changed by placing optical filters in front of the detectors. By analysis of the elastically scattered light

---

When this work was done, the authors were with Research Electro-Optics, 5505 Airport Boulevard, Boulder, Colorado 80301. M. Stephens (mstephen@ball.com) is now with Ball Aerospace & Technologies Corp., 1600 Commerce Street, Boulder, Colorado 80301.

Received 9 August 2002; revised manuscript received 7 March 2003.

0003-6935/03/193726-11\$15.00/0

© 2003 Optical Society of America

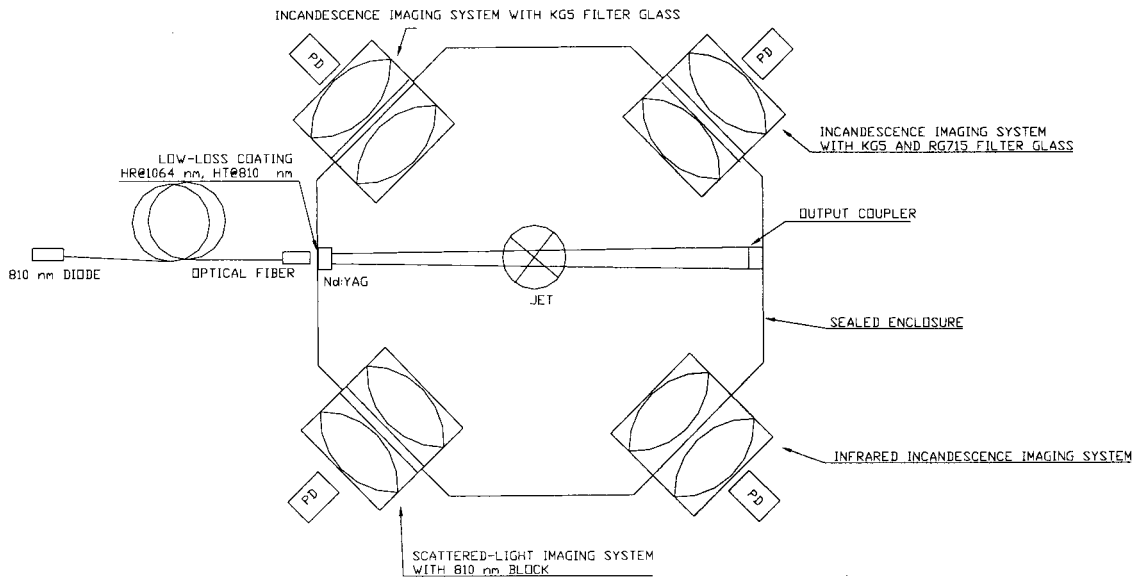


Fig. 1. Optical layout of the instrument. An interaction region is created by the intersection of a gas stream containing airborne particles (shown here with the gas jet perpendicular to the page) and the intracavity light of a high-finesse Nd:YAG laser. The particle is heated to incandescence as it is directed through the 1.064- $\mu\text{m}$  light, and both the elastically scattered light and the incandescent light are imaged by a variety of detectors.

(at 1.064  $\mu\text{m}$ ) the size of the particle at the time of vaporization can be determined. The abrupt termination of elastically scattered light verifies that the particle has been vaporized. Analysis of the LII over one or more spectral bandwidths provides the temperature of the particle during the vaporization process. The precise relationship between the temperature of the particle during vaporization and the composition of the particle is quite complex, but, to a good approximation, the particle's temperature reaches the boiling point of its constituent material while it is undergoing vaporization. This method therefore permits a straightforward determination of the particle's boiling point, which provides information about the composition of the particle. Elements such as tungsten, graphite, and silicon are easily separable. Airborne soot can also be detected and identified.

## 2. Apparatus

Figure 1 illustrates the optical layout. A diode-pumped Nd:YAG laser cavity is built into an aluminum block. A gas stream is focused through the center of the laser cavity with a concentric-nozzle jet system.<sup>23</sup> Test particles are introduced into the gas stream by a Particle Measuring Systems PG-100 nebulizer. The elastically scattered light and the incandescent light are imaged onto avalanche photodiodes (APDs) by four compound-lens systems. Data is taken with a digital oscilloscope and a desktop computer.

The 0.12-m-length Nd:YAG cavity consists of a 0.5-cm-thick Nd:YAG crystal and a mirror with a 0.3-m radius of curvature. Both surfaces of the crystal are superpolished flat. One side has a very-low-loss [ $<2$  parts per million (ppm)] multilayer dielectric coating

that has a high transmission at the wavelength of the diode pump light (0.81  $\mu\text{m}$ ) and very high reflectance ( $>99.99999\%$ ) at 1.064  $\mu\text{m}$ . The other surface is coated with a very-low-loss antireflection coating. The mirror is a high reflector with a leakage transmission of 15 ppm; the leakage through the mirror permits monitoring of the intracavity power. The  $\text{TEM}_{00}$  beam diameter at the center of the cavity is 500  $\mu\text{m}$ . The pump is an SDL 2362 multimode diode laser coupled to the cavity through an optical fiber. The circulating intensity at the center of the cavity is  $1.3 \times 10^6$  W at a pump power of 0.7 W.

The jet is a concentric-nozzle system. The airborne particles exit through the center nozzle with a flow of  $2.3 \times 10^{-6}$  to  $4.7 \times 10^{-6}$   $\text{m}^3/\text{s}$ . Gas exiting through the outer nozzle forms a sheath that focuses the airborne particles. The sheath flow is typically eight times greater than the nozzle flow. The jet can be translated perpendicular to and along the beam in order to align it directly over the center of the beam. Nonabsorbing polystyrene latex (PSL) spheres are used to align the jet by measuring the localization of the particles through comparison of the theoretical pulse-height distribution for localized particles with that measured with a multichannel analyzer. The waist of the particle stream is calculated from the pulse-height distribution of the PSL spheres and is typically half the laser beam's waist.

Each compound-lens assembly images light onto a single-element APD to form a single detection channel. There are four detection channels—one scatter channel for detection of the 1.064- $\mu\text{m}$  elastically scattered light and three incandescence channels. One lens assembly is designed to collect 1.064- $\mu\text{m}$  light with minimal aberrations. This assembly images the elastically scattered light onto a silicon APD

(EG&G C30724) and forms the scatter channel. Two other lens assemblies are designed to correctly image 0.300–0.800- $\mu\text{m}$  light. These assemblies also image light onto EG&G C30724 silicon APDs and form two separate visible incandescence channels. The fourth assembly collects 1.4–1.7- $\mu\text{m}$  light and images it onto a Judson J-16 germanium APD to form an infrared incandescence channel.

Filter glass can be inserted into the lens assemblies without distorting the image. The elastic-scattering detection channel contains 2-mm-thick Schott RG850 filter glass, which blocks the 0.81- $\mu\text{m}$  pump light but passes the 1.064- $\mu\text{m}$  scattered light. The filter glass in the 0.300–0.800- $\mu\text{m}$  incandescence imaging assemblies can be varied, but for the work presented here one channel contained 2-mm-thick Schott KG5 glass that transmits light from 0.310 to 0.770  $\mu\text{m}$ , which includes most of the light imaged by the system. The other channel contained 2-mm-thick Schott KG5 glass as well as a 2-mm-thick Schott RG715 glass, which transmits incandescent light only from 0.7 to 0.8  $\mu\text{m}$ . In the infrared imaging system a silicon lens acts as a filter so that no additional filter glass is necessary.

The APDs are attached to the lens assemblies and can be translated in three dimensions to optimize alignment. Each compound imaging system is built as a separate assembly and screws directly into the aluminum block. The assembly seals against the block with a Viton O-ring. The assemblies are easily interchangeable so that a variety of signals can be viewed simultaneously.

A LeCroy LC334A digital oscilloscope is triggered by the signal from the 1.064- $\mu\text{m}$  detection channel, and signals as a function of time from all four of the detectors are stored for a single particle. The data is then transferred to a desktop computer, and the incandescent signals are analyzed to determine the temperature of the particle when it vaporized. The scatter signal is analyzed to determine the size of the particle and to confirm that it vaporized. Pulse widths were typically 2–4  $\mu\text{s}$  and were typically recorded with a resolution of 0.01  $\mu\text{s}$ .

### 3. Theory

This particle-identification technique uses the magnitude and spectral dependence of the incandescence signal to determine the vaporization temperature of the incident particle. The composition of the particle is then inferred from the vaporization temperature. The size of the particle is inferred from the magnitude of the elastically scattered light. The vaporization and light detection processes can be modeled to determine the capabilities of the instrument. The time dependence of the particle radius and temperature can be solved numerically with the energy and mass balance equations for the laser-particle system.<sup>6,10,24,25</sup> A simpler model can be used to estimate the incandescence-detection limits of the instrument. Since the simpler model is useful for instrument design, this section will first describe a simplified steady-state model of the vaporization and

detection process, and then it will describe a more accurate, time-dependent model.

#### A. Simplified Model—Detection Limits

In the simplest model, the time dependence of the laser intensity incident on the particle and the internal heating of the particle are ignored. The system is assumed to be in a steady state in which the absorbed energy is balanced by the energy lost due to heat conduction through the surrounding air. A simple expression relating the laser intensity to the vaporization of a particle of a given radius ( $\alpha$ ), boiling point ( $T_b$ ), and absorption coefficient ( $K_{\text{abs}}$ ) can be determined:

$$K_{\text{abs}}\pi\alpha^2I - h_N(T_b - T_0)\pi\alpha^2 = 0, \quad (1)$$

where  $T_0$  is the ambient temperature of the unheated air,  $I$  is the incident laser intensity, and  $h_N$  is the Nusselt number and is approximately equal to  $k_{\text{air}}/\alpha$ ,<sup>26</sup> where  $k_{\text{air}}$  is the thermal conductivity of air. The first term represents the rate of the particle's energy absorption from the laser. The second term represents the rate of the particle's energy loss by heat conduction through the surrounding air. When more light is absorbed by the particle than is lost to conduction, the particle heats up until it begins to vaporize. Although this approximation ignores internal heating of the particle and vaporization of the particle, it is adequate for estimating the limiting factors for vaporizing particles in a given system. When the time dependence of the system is added, a higher intensity than predicted by Eq. (1) is needed to vaporize a particle with a given radius and absorption coefficient. For the system described in Section 2 the simplified model predicts vaporization intensities that are too low by a factor of four.

To determine the detection limits for a system using a single detector for the incandescent light, some assumptions must be made about the instrument itself. The magnitude of the incandescence signal depends on the particle's radius, boiling point, and emissivity ( $\epsilon$ ) in the spectral region over which the incandescence signal is detected. It also depends on the responsivity ( $\eta$ ) of the detector, the fraction of incandescent light collected by the imaging system ( $d\Omega$ ), and the fraction of incandescent light emitted over the spectral region of the detector ( $\Delta$ ). The signal-to-noise ratio is approximately equal to 1 when

$$d\Omega\Delta\eta\sigma_{\text{sb}}T_b^44\pi\alpha^2\epsilon = (N^2 + I_N^2)^{1/2}f, \quad (2)$$

where  $N$  is the detector amplifier's noise current,  $I_N$  is the photodetector's noise current, and  $f$  is the detector's bandwidth (in this case, the detector's bandwidth was approximated as the inverse of the minimum pulse width of a vaporizing particle).  $\Delta$  represents the fraction of incandescent light that is

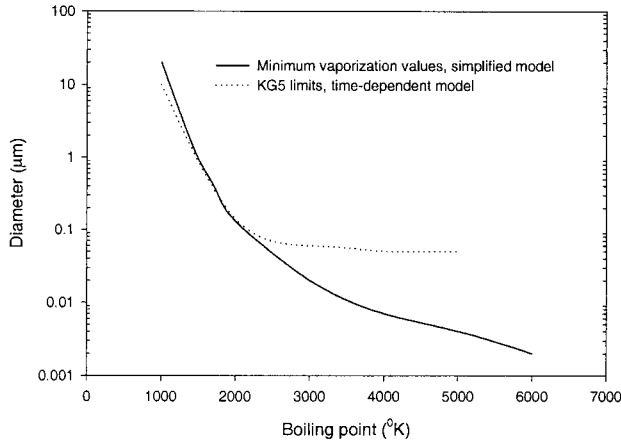


Fig. 2. Detection and vaporization limits of the system described in Section 3 for a particle with absorption coefficient and emissivity both constant and wavelength equal to 1. The limits are shown for an incandescence-detection channel using KG5 filter glass. The values used in the simplified model were  $N = 2 \times 10^{-12}$  A/Hz<sup>1/2</sup>,  $f = 1$  MHz,  $d\Omega = 0.16$ ,  $I_0 = 10^6$  W/cm<sup>2</sup>,  $k_{\text{air}} = 2.6 \times 10^{-4}$  W cm<sup>-1</sup> s<sup>-1</sup> K<sup>-1</sup>,  $\eta = 8$  W/A, and  $I_N = 10^{-12}$  A/Hz<sup>1/2</sup> for the silicon APD. The values used for the thermodynamic properties for the time-dependent model were the values for graphite ( $H_v = 7.8 \times 10^5$  J/mol,  $\rho_s = 2.62$  g/cm<sup>3</sup>,  $C_s = 0.72$  J g<sup>-1</sup> K<sup>-1</sup>,  $W_v = 36$  g/mol, and  $W_s = 12$  g/mol), with the exception of  $K_{\text{abs}}$ ,  $\epsilon$ , and  $T_b$ .  $K_{\text{abs}}$  and  $\epsilon$  were equal to 1, and  $T_b$  was varied from 1000 to 5000 K to determine the detection limits.

emitted in the spectral bandwidth of the incandescence detector (ibw),

$$\Delta = \frac{\int_{\text{ibw}} B(\lambda) d\lambda}{\int_0^\infty B(\lambda) d\lambda}, \quad (3)$$

where

$$B(\lambda) = \frac{2\epsilon\pi hc^2}{\lambda^5} \frac{1}{\exp(hc/\lambda kT) - 1} \quad (4)$$

is the blackbody radiation at  $T = T_b$ . In this simple approximation it is assumed that the emissivity is constant over the spectral bandwidth of the detector. Figure 2 shows the calculated detection and vaporization limits for the instrument, described in Section 2, that uses the broadband visible incandescence detection channel (KG5 filter glass). The detection limits for this instrument were not optimized for particles of any particular size or temperature. The detection limits can be optimized for specific particles through the choice of the spectral bandwidth of the incandescence detector, the design of the detection electronics, the circulating power inside the cavity, and modification of the jet (and therefore the pulse width of the signal).

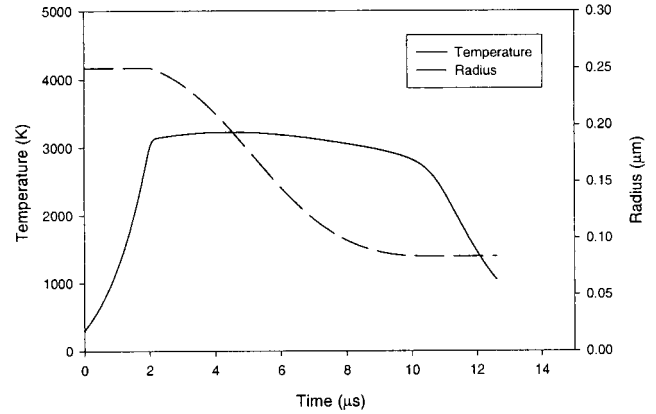


Fig. 3. Calculated temperature and radius for a graphite particle with an initial radius of 0.25  $\mu\text{m}$ .

### B. Time-Dependent Particle Heating and Vaporization

Differential equations for the temperature and radius of a particle can be derived from the time-dependent energy balance equation<sup>10,11</sup>:

$$K_{\text{abs}}(a)\pi a^2 I(t) - h_N(T - T_0)\pi a^2 - \frac{H_v}{W_v} \frac{dM}{dt} - \sigma_{\text{sb}} 4\pi a^2 (T^4 - T_0^4) = \frac{4}{3} \pi a^3 \rho_s C_s \frac{dT}{dt}, \quad (5)$$

where the terms represent the absorption of power from the laser, the rate of loss due to heat conduction away from the particle, the loss of energy due to vaporization of the particle, the energy loss due to blackbody radiation, and the rise in the internal temperature of the particle; the symbols are defined in Appendix A. Blackbody radiation is the smallest loss mechanism. It is typically 2 orders of magnitude smaller than the energy loss due to vaporization, which is the dominant energy-loss mechanism. The loss due to heat conduction is generally an order of magnitude smaller than the loss due to vaporization.

The absorption coefficient and the Nusselt number do not remain constant as the particle vaporizes. Expressions that approximate their dependence on the mass loss, particle temperature, and particle radius were developed and are described in Appendix B. Those relationships and the relationship between the radius of the particle and the mass loss,

$$\frac{da}{dt} = - \frac{dM}{dt} \frac{1}{4\pi\rho_s a^2}, \quad (6)$$

can be used to derive two coupled differential equations that can be solved numerically to find the temperature and radius of the particle as a function of time. Figure 3 shows the solutions of the coupled equations for a graphite particle with an initial radius of 0.25  $\mu\text{m}$ .

The magnitude and time dependence of the incandescence and scatter signals can now be calculated. The scatter signal,  $S_{\text{scat}}$ , can be calculated from Mie scattering. For a Rayleigh particle ( $a \ll \lambda/2\pi$ ) the

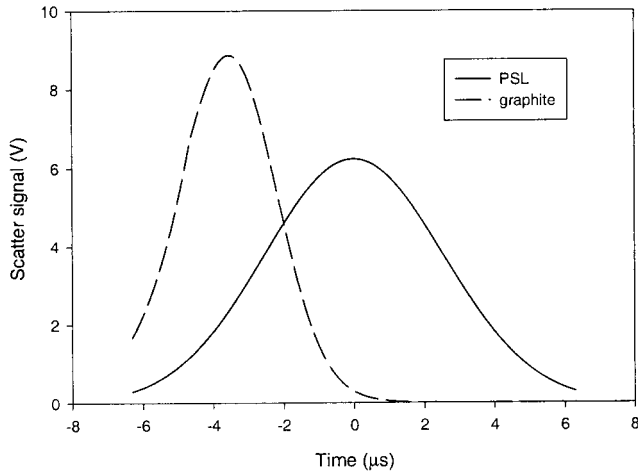


Fig. 4. Calculated normalized scatter signals from an absorbing particle (graphite) that vaporizes before passing completely through the laser light and a nonabsorbing particle (PSL) of the same initial diameter (0.5  $\mu\text{m}$ ). Note the reduced pulse width for the graphite particle, indicating that the particle vaporized before traversing the beam.

magnitude of the scatter signal is proportional to the incident laser intensity and the sixth power of the radius<sup>27</sup>:

$$S_{\text{scat}}(t) = \eta d \Omega I(t) \frac{8}{3} \pi a^6 \left( \frac{2\pi}{\lambda} \right)^4 \left| \frac{m^2 - 1}{m^2 + 2} \right|^2, \quad (7)$$

where  $m$  is the complex index of refraction of the particle. The radius of the particle can be calculated from the magnitude of the measured scattered light. If the particle's composition, and therefore the index of refraction, is unknown, a value for  $m$  must be assumed. The scatter signal for a nonabsorbing particle is a Gaussian pulse. Vaporization can be confirmed by measurement of the pulse width of the scatter signal. The strong dependence of the scatter signal on the particle's radius results in a measurably shorter pulse width when a particle vaporizes (Fig. 4). The signal,  $S_{\text{incand}}$ , from the incandescent power that reaches the detector is

$$S_{\text{incand}}(t) = \varepsilon 4 \pi a(t)^2 d \Omega \int_0^\infty B[\lambda, T(t)] R(\lambda) \eta(\lambda) d\lambda, \quad (8)$$

where  $R(\lambda)$  is the transmission of the filter glass in the incandescence-detection channel. The temperature of the particle when it vaporizes can be calculated from the incandescence signal, and the particle's radius can be derived from the scatter signal. The initial value of the scatter signal provides an initial radius for the particle. Equation (8) can then be used to calculate the temperature from  $S_{\text{incand}}$ . To do so, one must assume the particle's emissivity. An alternative method for calculating the temperature that does not rely on an assumption of a value for the emissivity is to use two-color

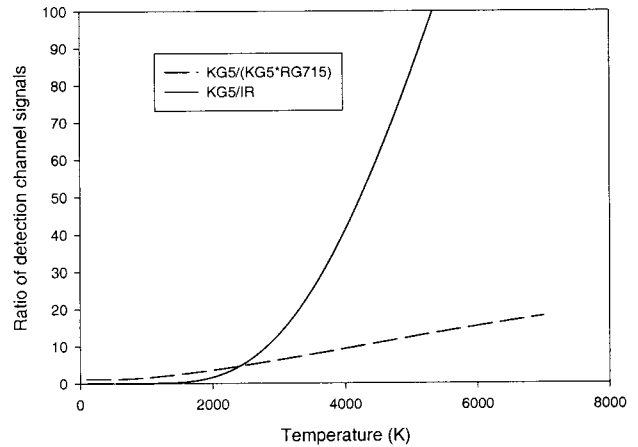


Fig. 5. Calculated ratio of signals from the incandescent-detection channels as a function of boiling point. It is assumed that the emissivity is wavelength independent. Two plots are shown—one shows the ratio of signals from the two visible detection channels (KG5 and KG5\*RG715 filter glasses), while the other shows the ratio of the broadband visible channel (KG5 filter glass) to the infrared channel.

pyrometry and take the ratio of the maximum value of the incandescence signals from two detectors with different spectral bandwidths. This method uses the more reliable assumption that the emissivity is constant with wavelength over the detection bandwidth and also removes the dependence of the signal on the radius of the particle. The detection limits for a single channel with KG5 filter glass, calculated with the time-dependent model, are shown in Fig. 2. The calculated values for the ratio of detection channel signals as a function of boiling points are shown in Fig. 5.

### C. Limits and Applicability of Model

The design of this detection method focuses on characterization of the boiling point of airborne particles with a diameter in the range of 0.05–1  $\mu\text{m}$ . The composition of the particle is inferred from the boiling-point data. Therefore, by design, particles of different composition but with similar boiling points will be indistinguishable. However, in many situations, such as clean-room detection, where some information about the type of airborne particles is available, the discrimination between absorbing and nonabsorbing particles and particles with high and low boiling points is useful and allows discrimination between, for example, plastic and metallic particles.

The model used assumes that the particles are spherical, that they have a radius much less than the wavelength, that their thermodynamic values, such as specific heat, are constant with temperature; that they do not melt before vaporizing, and that their emissivity is constant with wavelength. Deviation from these assumptions typically leads to only a small increase in the uncertainty of the measurement.

Aspherical particles can change the magnitude of the incandescence signal since that signal depends on

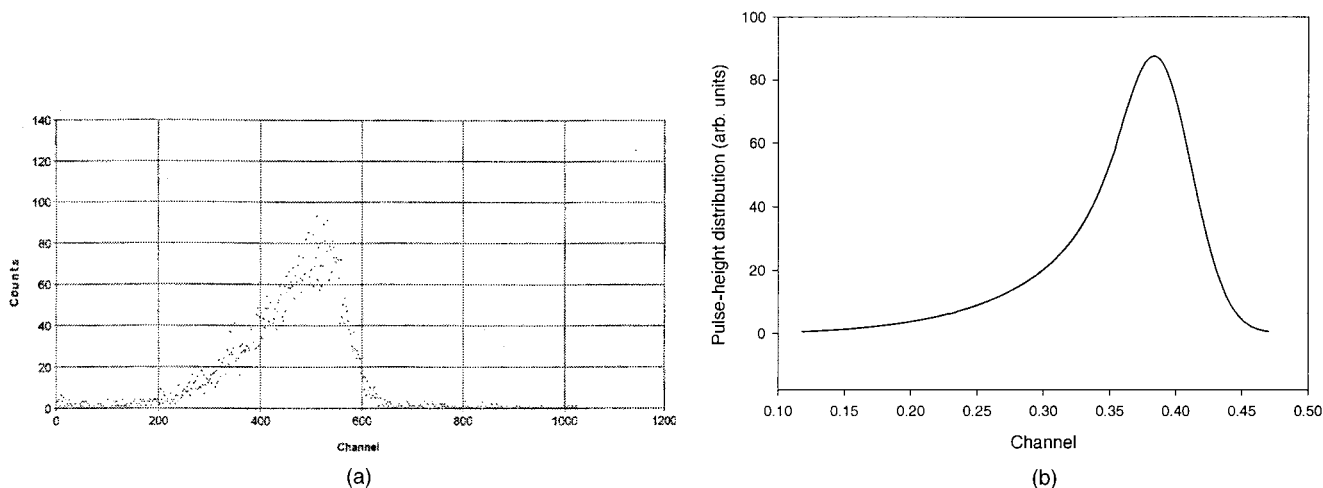


Fig. 6. (a) Pulse-height distributions measured with a multichannel analyzer of 0.304- $\mu\text{m}$  PSL particles. (b) Calculated distribution for particles localized to half the laser beam's waist size.

the surface area of the particle. The magnitude of the elastically scattered light from an aspherical particle does not follow from Eq. (7). The magnitude of the scattered light will depend on the orientation of the particle relative to the incident light. The scattering cross section for an oblate spheroid can vary from 0.5 to 2.5 times the cross section for a sphere with a radius the same length as the spheroid's semi-axis.<sup>27</sup> Because of the  $a^6$  dependence of the elastic cross section, a factor-of-two difference in the magnitude of the elastically scattered signal will lead to only a 16% error in the value of the radius of the particle calculated from Eq. (7). This level of accuracy for sizing particles is still of use in many applications, such as clean-room contamination monitoring.

The variation in the particle's specific heat with temperature affects the time dependence of the particle's temperature but does not change the maximum temperature the particle reaches. The dominant physical quantity for determining the maximum particle temperature is the boiling point itself. Similarly, if the particle melts before vaporizing, the thermodynamics properties will change,<sup>28</sup> but the most important physical quantity is still the boiling point of the material.

The emissivity can also change with temperature.<sup>28</sup> This will affect the accuracy of the temperature measurement by a small amount. For a particle with a relatively high emissivity ( $>0.75$ ) the effect is of the order of 5–10%. For example, the correction for radiation pyrometer readings for a metal particle with an emissivity of 0.85 at 1800 K is 90 K.<sup>28</sup> If the emissivity is constant with wavelength and two-color pyrometry is being used, the effect is not important. The variation of the emissivity with wavelength, however, can still result in an incorrect value of the particle's temperature. In particular, the difference between the emissivity over an infrared bandwidth and the visible bandwidth may be significant, and care should be taken when choos-

ing spectral regions for two-color pyrometry. Copper, for example, has an emissivity of 0.1 at 1.0  $\mu\text{m}$  and 0.56 at 0.5  $\mu\text{m}$ .<sup>28</sup>

Finally, this model assumes that the particle heats uniformly and instantaneously. This assumption is valid since the relevant time scales for internal equilibration are short compared with the time scale for heating to vaporization. The time for heat to diffuse across the particle is

$$\tau_{\text{diff}} = \frac{\rho_s C_s a^2}{4\kappa_s}, \quad (9)$$

where  $\kappa_s$  is the thermal conductivity of the particle.<sup>25</sup> For a typical metal,  $\rho_s \sim 10 \text{ gm/cm}^3$ ,  $C_s \sim 0.4 \text{ J g}^{-1} \text{ K}^{-1}$ , and  $\kappa_s \sim 1 \text{ W cm}^{-1} \text{ K}^{-1}$ , so  $\tau_{\text{diff}} \sim 2.5 \times 10^{-9} \text{ s}$  for a 1.0- $\mu\text{m}$ -diameter particle. The time scale for vaporization with the apparatus described in Section 2 is  $\sim 10^{-6} \text{ s}$ .

#### 4. Experimental Results and Discussion

PSL microspheres were used for the initial alignment of the jet and to calibrate the elastic-scattering detection channel. By measuring the pulse-height distribution of the elastically scattered light, it was determined that the PSL spheres were localized with a waist size close to half the laser beam's waist size [Fig. 6(a)–6(b)]. The magnitude of the signal from a 0.304- $\mu\text{m}$ -diameter sphere was used in conjunction with Eq. (7) to calibrate the collection efficiency of the lens assembly and the response of the photodetector. This calibration was then used with Eq. (7) to determine the size of other particles from the scattered light signal.

##### A. Demonstration of Empirical Differentiation between Materials

Vaporization temperatures were derived from two-color pyrometry for a variety of metals. For these measurements two incandescence channels were used. One lens assembly had 2-mm-thick Schott

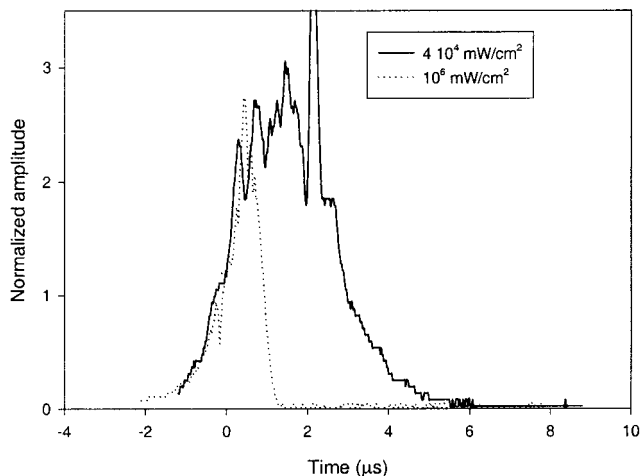


Fig. 7. Normalized signal from the elastically scattered light for graphite at two circulating intensities. Note that the particle vaporizes more quickly at the higher intensity, resulting in reduction in the pulse width of the scattered signal. The signal from the particle vaporized at low circulating intensity shows both the poor signal-to-noise ratio caused by the reduction in circulating intensity and fluctuations in the signal that we attribute to non-spherical particles.

KG5 filter glass that transmits wavelengths from 0.310 to 0.770  $\mu\text{m}$ . The other assembly had 2-mm-thick Schott KG5 filter glass and a 2-mm-thick Schott RG715 filter glass. This combination of glass transmits wavelengths from 0.7 to 0.8  $\mu\text{m}$ . Sample particle suspensions were prepared by mixing commercially available finely powdered metals with deionized water and were introduced into the jet's gas stream with a Particle Measuring Systems PG-100 nebulizer. A digital oscilloscope captured a single event by triggering on the signal from the detector for elastically scattered light. The maximum values from both incandescent channels and the scatter channel were transferred to a personal computer.

The pulse width of the scatter signal was also measured and transferred to the personal computer. If the pulse width was less than the pulse width of a PSL particle, it was determined that the particle had vaporized (Fig. 7), and the ratio of the two incandescent values was compared with a model to determine the temperature of the particle at vaporization (Fig. 5). An alternative method for determining whether the particle vaporized was also tested. In this method a split photodetector was used to detect the elastically scattered light. The detector was aligned so that the signals on both halves of the detector were equal when a nonabsorbing PSL particle passed through the laser beam. When an absorbing particle vaporized, the signals on the detectors were unbalanced and vaporization was confirmed.

The size of the particle was determined from the maximum value of the elastically scattered signal by using Eq. (7) with  $I(t) = I(0)$ . Since the particle typically vaporizes before reaching the center of the beam and therefore before reaching the maximum

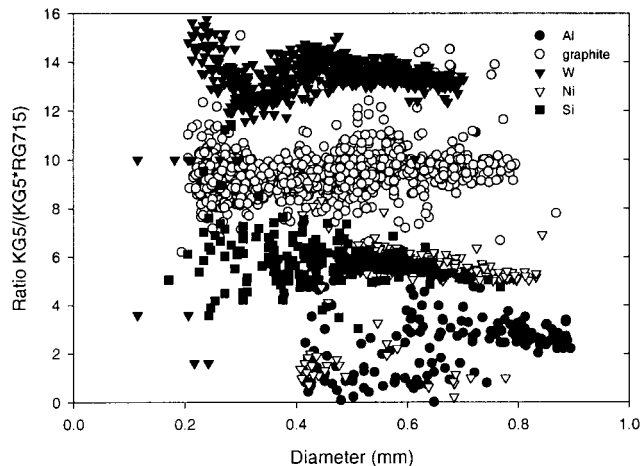


Fig. 8. Demonstration of the ability of this instrument to distinguish between different metals. The left axis shows the ratios of the maximum values in the two incandescence detectors, and the right axis shows the corresponding temperatures for particles with emissivities of 1 over the detection bandwidth.

circulating intensity, to calculate a more accurate value for the particle's diameter, one could measure the rise time,  $t_r$ , of the scatter signal and use Eq. (A5) in Appendix A to calculate  $I(t = -t_r)$ . However, because of the  $a^6$  dependence of the scattered light, this correction for the data taken with this apparatus was typically less than 10% of the calculated radius. Another source of error in the particle sizing is due to the assumption that the particle's diameter is much less than the wavelength of light, a condition that was not always true for some of the materials used.

The value of the scattering cross section depends on the complex index of refraction for the metal and is different for different materials. If the composition of the particle is unknown or the complex index of refraction is unknown, no correction can be made to the scattering cross section. For these measurements the scattering cross section for PSL spheres was used, which led to an estimated 30% uncertainty in the size of the particle.

Figure 8 shows the results of two-color pyrometry for tungsten ( $T_b = 5828$  K),<sup>29</sup> graphite ( $T_b \sim 4200$  K),<sup>30</sup> silicon ( $T_b = 3540$  K),<sup>29</sup> nickel ( $T_b = 3187$  K),<sup>29</sup> and aluminum ( $T_b = 2794$  K).<sup>29</sup> Nickel and silicon, which have similar boiling points, are not distinguishable from each other, while the other elements are easily distinguishable. Note that aluminum appears to have a vaporization point lower than 2794 K. This is probably due to its drop in emissivity over the RG715 bandwidth.<sup>31</sup> This may also explain the slight difference between the expected and measured vaporization temperatures of silicon and nickel.

#### B. Measurements of Graphite; Detailed Comparison to Model

In the previous section the capability of this instrument for discriminating between particles of unknown composition was demonstrated. In this

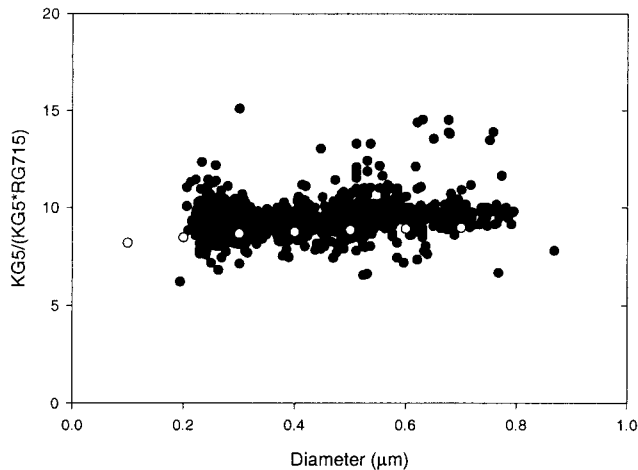


Fig. 9. Results of two-color pyrometry on graphite and comparison with calculated values (shown as open circles).

section measurements of graphite are compared with the predictions of the model. The absorption coefficients and elastic-scattering cross sections are calculated from published values for the complex indices of refraction.<sup>32</sup> We were unable to obtain graphite particles with a known size distribution, so the size of the particle is inferred from the complex index of refraction and Eq. (7).

Figure 9 shows the results of two-color pyrometry on graphite and compares the model's predictions with the data. The values for the  $KG5/(KG5*RG715)$  ratios compare well. Figure 10 shows how absolute values of the KG5 signal alone compare with the model. Using a single incandescence channel is an option if one either knows the emissivity of the particle to be detected or is willing to assume a value for the emissivity of a particle of unknown composition. The values used in the model were  $H_v = 7.8 \times 10^5$  J/mol,  $\rho_s = 2.62$  g/cm<sup>3</sup>,  $C_s = 0.72$  J g<sup>-1</sup> K<sup>-1</sup>,  $W_v = 36$  g/mol,  $W_s = 12$  g/mol,  $K_{abs} = 1$ , and  $\epsilon = 1$ .

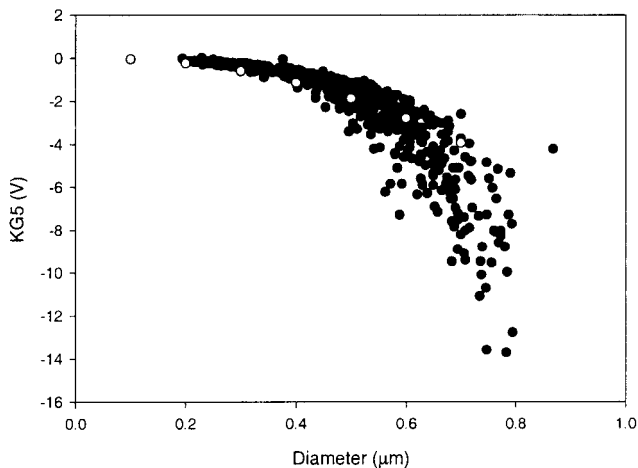


Fig. 10. Comparison of model predictions (shown as open circles) to KG5 signal alone for graphite.

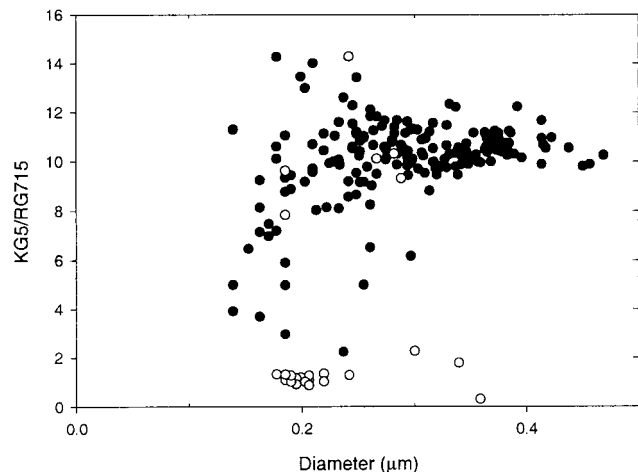


Fig. 11. Detection of soot using the LII method in a solid-state laser cavity. The open circles show the counts taken while sampling room air for 13 min. The closed circles show the counts taken with an oil lamp burning near the intake valve for 13 min.

### C. Detection of Atmospheric Aerosols

One possible application for this measurement technique is air pollution monitoring. Common airborne pollutants include silicon, sulphur, oxides and nitrides of metals, and soot.<sup>21</sup> We have already shown the capability of this instrument to differentiate between various metals, including silicon and graphite. Soot detection, in particular, is ideal for this application because of soot's high absorption coefficient (1.064 μm). Filippov *et al.*<sup>21</sup> have shown that LII can be used to detect soot particles in air, however, that work assumed that the majority of the emission was due to soot particles, whereas this technique ensures that the emission is due to soot particles by measuring the vaporization temperature of the aerosol.

To demonstrate the capability of this instrument, ambient air was introduced into the cavity through the jet, then a burning oil lamp was placed underneath the intake. Figure 11 shows the result. The soot from the lamp is clearly detectable.

Soot particles may form loose agglomerates.<sup>21</sup> This leads to the questions of whether the particles break apart during vaporization and how that might affect this measurement technique. Following the arguments of Filippov *et al.*,<sup>21</sup> the soot particles can be expected to disintegrate when the laser intensity is strong enough to induce electrostatic breakdown between the agglomerated particles. Charge buildup due to thermionic emission of the hot particle overcomes the van der Waals attraction that holds the aggregates together. Using the model outlined by Filippov *et al.*,<sup>21</sup> it is expected that any aggregates will disintegrate soon after entering the laser beam.

## 5. Discussion

The fundamental limit of the incandescence-detection method will depend on the choices of the spectral-detection bandwidths for the incandescence channels, the electronic bandwidth of the detection

channels, and the numerical aperture of the imaging system. The electronic bandwidth of the detection channels is determined by the minimum pulse width of the incandescent signal. The speed with which the particle vaporizes depends weakly on the speed at which the particle is moving through the beam (i.e., the flow rate of the jet) and strongly on the intensity incident on the particle. The simple model described in Section 3 can be useful for adjusting these parameters to optimize the instrument design for the desired particle size and boiling point.

The temperature resolution of the incandescence-detection method also depends on the choices of the spectral-detection bandwidths for the incandescence channels as shown in Fig. 5. Additionally, it depends on the repeatability of the signal, which depends on the localization of the particles in the gas stream, the roundness of the particles, and the surface emissivity of the particles, which may change with oxidation.<sup>28</sup>

This demonstration has shown that very simple assumptions can be made for the index of refraction and the emissivity for particles of unknown composition while still providing useful information. Even if the index of refraction is unknown, the particle size can be approximated from Eq. (7) by using the index of refraction of PSL. Because of the  $a^6$  dependence of the magnitude of the elastically scattered signal, in the determination of size the error arising from a lack of knowledge of the index of refraction will be within 30–50%, even for particles with a very high index of refraction. The use of two incandescence-detection channels and two-color pyrometry can minimize the effect of an unknown emissivity, especially if the emissivity is constant with wavelength. The choice of the spectral filters for the two incandescence channels is a trade-off between temperature resolution (a large separation between filter transmission bands leads to greater resolution) and minimizing the effects of a wavelength-dependent emissivity (a large separation between filter transmission bands may decrease the accuracy of the temperature determination if the emissivity is strongly dependent on wavelength).

## 6. Conclusions

This work has demonstrated that rudimentary particle sizing and identification can be performed *in situ* with a combination of LII and elastic-scattering detection. Despite many simplifying assumptions, a number of materials that are relevant to clean-room and air pollution monitoring can be detected and differentiated, making this a viable technique for real-time aerosol measurements.

### Appendix A: Detailed Description of $K_{\text{abs}}$ , $h_N$ , and $I$

The absorption coefficient can be calculated exactly from the Mie equations<sup>27</sup> if the complex indices of refraction for the particle are known. To simplify

the model used here, the absorption coefficient was approximated with the empirical function

$$K_{\text{abs}} \cong \frac{2}{\pi} Q_{\text{abs}} \tan^{-1} \frac{a}{a_{\text{depth}}}, \quad (\text{A1})$$

where  $a_{\text{depth}}$  represents an absorption depth for 1.064- $\mu\text{m}$  light and  $Q_{\text{abs}}$  is the absorption coefficient for particles much larger than the absorption depth. The values for  $a_{\text{depth}}$  and  $Q_{\text{abs}}$  were assigned by solving the Mie equations at a few radii and using the values to fit the function in Eq. (6).

In this model the Nusselt number used in the simplified model is modified to include the effects of evaporation<sup>26</sup>:

$$h_N \cong \frac{2K_{\text{air}}}{a} \left( 1 + \frac{\frac{dM}{dt} C_{\text{air}}}{8\pi a k_{\text{air}}} + \frac{\frac{dM}{dt} C_{\text{air}}}{24\pi a k_{\text{air}}} \right)^{-1}. \quad (\text{A2})$$

The mass lost because of evaporation diffuses away from the particle at a rate<sup>26</sup>

$$\frac{dM}{dt} = \frac{4\pi a P_p D W_v 10^{-6}}{RT} \ln \left( 1 - \frac{P_p - P_{\text{atm}}}{P_p + P_{\text{atm}}} \right)^{-1}, \quad (\text{A3})$$

where  $P_p = P^* \exp[H_v(T - T_b)/RTT_b]$  is the partial pressure of the vapor from the particle<sup>10,26</sup> and

$$D = 2 \left( \frac{10^7 2k T N_A}{\pi W_v} \right)^{1/2} k T 10^6 (\pi d_{\text{air}}^2 P_{\text{atm}})^{-1} \quad (\text{A4})$$

is the diffusion coefficient for vapor from the particle in air.<sup>33</sup>

Because of the Gaussian profile of the intracavity laser light, the intensity ( $I$ ) of the light incident on the particle is also a function of time and can be written (assuming a straight-line trajectory through the center of the beam) as

$$I = I(t) = \frac{P_{\text{IC}} 10^{-3}}{\pi w_0^2} \exp \left( -\frac{t^2}{t_0^2} \right). \quad (\text{A5})$$

### Appendix B: Nomenclature

- $a$ , particle radius (cm).
- $a_{\text{depth}}$ , absorption depth (cm) (obtained from a fit to the solution of the Mie equations).
- $B(\lambda)d\lambda$ , blackbody radiation ( $\text{W m}^{-2} \text{sr}^{-1}$ ).
- $c$ , speed of light (m/s).
- $C_{\text{air}}$ , specific heat of air at 300 K ( $\text{J g}^{-1} \text{K}^{-1}$ ).
- $C_s$ , specific heat of the particle ( $\text{J g}^{-1} \text{K}^{-1}$ ).
- $D$ , diffusion coefficient in air for vapor from the incandescing particle ( $\text{cm}^2/\text{s}$ ).
- $d_{\text{air}}$ , diameter of air molecule (cm).
- $dM/dt$ , mass loss due to particle vaporization (g/s).
- $d\Omega$ , fraction of emitted light that is collected by the detection system.
- $\Delta$ , fraction of blackbody radiation emitted in the spectral band of the incandescence detector.
- $\varepsilon$ , emissivity at incandescence wavelengths.
- $f$ , photodetector amplifier bandwidth (Hz).
- $h$ , Planck's constant (J s).

$h_N$ , Nusselt number ( $\text{W cm}^{-2} \text{K}^{-1}$ ).  
 $H_v$ , latent heat of vaporization ( $\text{J/mol}$ ).  
 $I$ ,  $1.064\text{-}\mu\text{m}$  intensity ( $\text{W/cm}^2$ ).  
 $I_N$ , photodetector noise current ( $\text{A/Hz}^{1/2}$ ).  
 $\kappa_s$ , thermal conductivity of particle ( $\text{W cm}^{-1} \text{K}^{-1}$ ).  
 $k$ , Boltzmann's constant ( $\text{J/K}$ ).  
 $K_{\text{abs}}$ , Mie absorption coefficient at  $1.064 \mu\text{m}$ .  
 $k_{\text{air}}$ , thermal conductivity of air at  $300 \text{K}$  ( $\text{W cm}^{-1} \text{K}^{-1}$ ).  
 $\lambda$ , wavelength of emitted light ( $\text{m}$ ).  
 $m$ , complex index of refraction of particle.  
 $\eta$ , photodetector responsivity ( $\text{A/W}$ ).  
 $N$ , photodetector amplifier noise ( $\text{A/Hz}^{1/2}$ ).  
 $N_A$ , Avogadro's number.  
 $P_{\text{atm}}$ , local atmospheric pressure ( $\text{N/m}^2$ ).  
 $P_{\text{IC}}$ , intracavity power ( $\text{mW}$ ).  
 $p_0$ , power leaving the cavity ( $\text{mW}$ ).  
 $P_p$ , partial pressure of vapor from the incandescing particle ( $\text{N/m}^2$ ).  
 $P^*$ , reference pressure ( $\text{N/m}^2$ ).  
 $Q_{\text{abs}}$ , absorption coefficient at  $1.064 \mu\text{m}$  for large particle radius (obtained from a fit to the solution of the Mie equations).  
 $\rho_s$ , density of the particle in the solid phase ( $\text{g/cm}^3$ ).  
 $R$ , ideal gas constant ( $\text{J K}^{-1} \text{mol}^{-1}$ ).  
 $R(\lambda)$ , spectral bandwidth of incandescence detector.  
 $S_{\text{incand}}$ , signal from incandescence photodetector.  
 $\sigma_{\text{sb}}$ , Stefan-Boltzmann constant ( $\text{W cm}^{-2} \text{K}^{-4}$ ).  
 $T_b$ , boiling point at reference pressure  $P^*$  ( $\text{K}$ ).  
 $T_0$ , ambient air temperature ( $\text{K}$ ).  
 $T_{\text{OC}}$ , transmission of the cavity output coupler (ppm).  
 $t_0$ , pulse width of the scatter signal produced by a nonabsorbing particle (s).  
 $t_r$ , rise time of the elastically scattered signal (s).  
 $W_{\text{air}}$ , molecular weight of air ( $\text{g/mol}$ ).  
 $w_0$ ,  $1/e^2$  radius of beam intensity where particles pass through it (cm).  
 $W_v$ , molecular weight of the vapor from the incandescing particle ( $\text{g/mol}$ ).

The authors thank Rick Gallant for the optical imaging system design, Gerry Everett for the mechanical design, and Quentin Turchette for his review of the manuscript.

## References

- L. Fabiny, "Sensing rogue particles with optical scattering," *Opt. Photon. News*, January 1998, pp. 34–38.
- R. G. Knollenberg, "The measurement of latex particle sizes using scattering ratios in the Rayleigh scattering size range," *J. Aerosol Sci.* **20**, 331–345 (1989).
- W. D. Reents, S. W. Downey, A. B. Emerson, A. M. Muijsce, A. J. Muller, D. J. Siconolfi, J. D. Sinclair, and A. G. Swanson, "Single particle characterization by time-of-flight mass spectrometry," *Aerosol Sci. Technol.* **23**, 263–270 (1995).
- P. J. McKeown, M. V. Johnston, and D. M. Murphy, "On-line single-particle analysis by laser desorption mass spectrometry," *Anal. Chem.* **63**, 2069–2071 (1991).
- J. Gelbwachs and M. Birnbaum, "Fluorescence of atmospheric aerosols and lidar implications," *Appl. Opt.* **12**, 2443–2447 (1973).
- C. J. Dasch, "Continuous-wave probe laser investigation of laser vaporization of small soot particles in a flame," *Appl. Opt.* **23**, 2209–2215 (1984).
- S. Will, S. Schraml, K. Bader, and A. Leipertz, "Performance characteristics of soot primary particle size measurements by time-resolved laser-induced incandescence," *Appl. Opt.* **37**, 5647–5658 (1998).
- R. L. Vander Wal, "Laser-induced incandescence: detection issues," *Appl. Opt.* **35**, 6548–6559 (1996).
- R. L. Vander Wal and D. L. Dietrich, "Laser-induced incandescence applied to droplet combustion," *Appl. Opt.* **34**, 1103–1107 (1995).
- L. A. Melton, "Soot diagnostics based on laser heating," *Appl. Opt.* **23**, 2201–2208 (1984).
- A. C. Eckbreth, "Effects of laser-modulated particulate incandescence on Raman scattering diagnostics," *J. Appl. Phys.* **48**, 4473–4479 (1977).
- C. J. Dasch, "Spatially resolved soot-absorption measurements in flames using laser vaporization of particles," *Opt. Lett.* **9**, 214–215 (1984).
- R. L. Vander Wal and K. J. Weiland, "Laser-induced incandescence: development and characterization towards a measurement of soot-volume fraction," *Appl. Phys. B* **59**, 445–452 (1994).
- R. L. Vander Wal and K. A. Jensen, "Laser-induced incandescence: excitation intensity," *Appl. Opt.* **37**, 1607–1616 (1998).
- J. R. Fincke, C. L. Jeffery, and S. B. Englert, "In-flight measurement of particle size and temperature," *J. Phys. E* **21**, 367–370 (1998).
- E. A. Rohlffing and D. W. Chandler, "Two-color pyrometric imaging of laser-heated carbon particles in a supersonic flow," *Chem. Phys. Lett.* **170**, 44–50 (1990).
- T. Joutsenoja, J. Stenberg, R. Hernberg, and M. Aho, "Pyrometric measurement of the temperature and size of individual combusting fuel particles," *Appl. Opt.* **36**, 1525–1535 (1997).
- J. R. Fincke, W. D. Swank, C. L. Jeffery, and C. A. Mancuso, "Simultaneous measurement of particle size, velocity, and temperature," *Meas. Sci. Technol.* **4**, 559–565 (1993).
- T. Joutsenoja and R. Hernberg, "Pyrometric sizing of high-temperature particles in flow reactors," *Appl. Opt.* **37**, 3487–3493 (1998).
- P. Roth and A. V. Filippov, "In situ ultrafine particle sizing by a combination of pulsed laser heatup and particle thermal emission," *J. Aerosol Sci.* **27**, 95–104 (1996).
- A. V. Filippov, M. W. Markus, and P. Roth, "In-situ characterization of ultrafine particles by laser-induced incandescence: sizing and particle structure determination," *J. Aerosol. Sci.* **30**, 71–87 (1999).
- R. L. Vander Wal, T. M. Ticich, and J. R. West, Jr., "Laser-induced incandescence applied to metal nanostructures," *Appl. Opt.* **38**, 5867–5879 (1991).
- R. A. Keller and N. S. Nogar, "Gasdynamic focusing for sample concentration in ultrasensitive analysis," *Appl. Opt.* **23**, 2146–2151 (1984).
- F. A. Williams, "On vaporization of mist by radiation," *Int. J. Heat Mass Transfer* **8**, 575–587 (1965).
- R. L. Armstrong, "Interactions of absorbing aerosols with intense light beams," *J. Appl. Phys.* **56**, 2142–2153 (1984).
- C. A. Sleicher and S. W. Churchill, "Radiant heating of dispersed particles," *Ind. Eng. Chem.* **48**, 1819–1824 (1956).
- H. C. van de Hulst, *Light Scattering by Small Particles* (Dover, New York, 1991).
- C. J. Smithells, *Metals Reference Handbook*, 4th ed. (Butterworths, London, 1967).
- Periodic Table of the Elements*, produced by Sargent-Welch Scientific Company, Skokie, Ill., 1980.

30. F. P. Bundy, "Pressure-temperature phase diagram of elemental carbon," *Physica A* **156**, 169–178 (1989).
31. R. A. Paquin, "Properties of metals," in *Handbook of Optics*, M. Bass, E. W. Van Stryland, D. R. Williams, and W. L. Wolfe, eds. (McGraw-Hill, New York, 1995), Vol. 2, pp. 35–49.
32. B. M. Vaglieco, F. Beretta, and A. D'Alessio, "In situ evaluation of the soot refractive index in the UV-visible from the measurement of the scattering and extinction coefficients in rich flames," *Combust. Flame* **79**, 259–271 (1990).
33. J. F. O'Hanlon, *A User's Guide to Vacuum Technology*, 2nd ed. (Wiley, New York, 1989).